Periodic Nanopillar N-I-P Amorphous Si Photovoltaic Cells Using Carbon Nanotube Scaffolds

Hang Zhou, Fei Tao, Pritesh Hiralal, Arman Ahnood, Husnu Emrah Unalan, Arokia Nathan, *Fellow, IEEE*, and Gehan A. J. Amaratunga

***Abstract*—Arrays of periodic one-dimensional nanomaterials offer tunable optical properties in terms of light–matter interaction which are attractive for designing efficient optoelectronic devices. This paper presents a fabrication of bottom-up grown nanopillar (NP) array solar cells based on n-i-p thin-film amorphous silicon using scaffolds of vertically aligned carbon nanotube (CNT) array. The effects of varying the CNT spacing over the range from 800 to 2000 nm on optical and electrical properties of the solar cells were investigated. The NP solar cell with CNT spacing of 800 nm exhibited 'moth-eye' broadband antireflection behavior, showing an average reflectance value lower than 10%. The enhanced optical absorption translated to significant enhancements in photocurrent and quantum efficiency compared to a conventional planar solar cell under low light condition. The open-circuit voltage (V_{oc}) of the NP solar cell was found systematically correlated with the CNT spacing and the illumination condition. The results presented here is of importance for developing high efficiency one-dimensional nanostructured solar cells.**

***Index Terms*—Amorphous silicon, carbon nanotube (CNT), nanophotonics, nanostructured materials, photovoltaic cells.**

I. Introduction

INTERACTION of light with spatially ordered nanostructures exhibits some unique characteristics, particularly when the features sizes are in the order of the incident wavelength. Exploiting these properties to enhance the absorption of solar cells has been an active research topic over the last few years [1]–[4]. One category of such nanostructures are one dimensional nanowire(NW)/nanopillar(NP) structure which offers superior optical absorption enhancement through control of its diameter, length, and the resulting array density and pattern [5], [6]. NW/NP structures are attractive not only for solar cells but also for other applications such as large area photodetectors and image sensors, e.g., for medical imaging [7]. Furthermore, the radial junction geometry decouples the light absorption direction and the charge collection by virtue of their orthogonal directions, enabling high optical absorption through the use of long NWs whilst minimizing photogenerated carrier losses through the use of thin absorber layers [8]. These NW/NP structures, when carefully designed, can also provide excellent broadband optical absorption enhancement for light with wide incidence [9]–[12]. The bottom up growth method for one dimensional nanomaterials such as carbon nanotubes (CNTs) [13], [14], silicon NWs [15], [16], and zinc oxide NWs [17]–[19] has already been adopted to fabricate nanostructured interconnects, transistors, and photovoltaic (PV) devices. Demonstrated devices range from ZnO (shell)/Si (core) radial heterojunction NW photodiode [20], [21], core/shell Si NW array solar cells [21], [22] to CNT/amorphous Si coaxial cable-like NW solar cells [24], [25]. These devices exhibit higher photoresponsivity and enhanced short circuit current compared to their planar counterparts. This effect can be further enhanced through the use of periodic structures, such as sub-wavelength gratings [26] and NW arrays [27], [28] based devices with superior photon capturing efficiencies have been demonstrated. Nevertheless, in terms of solar cell efficiencies, the bottom up techniques, with reported values of 5–6% [22]–[25], still lag behind the top down etched techniques. Indeed the best reported efficiency of top-down etched Si NP solar cells is 18.2% [29]. Therefore, it is important to further investigate the fundamental problems with the bottom-up grown NW solar cells, such as examining the effect of geometrical parameters on the device performance, including array density and periodicity.

This paper attempts to systematically investigate the fundamental limitations of the bottom-up grown NP solar cells through examining the effect of geometrical features of the NW array on the optical and electrical characteristics of PV devices. In particular, the emphasis on the solar cell design is to capture energy from low intensity light when limited area is available, conditions typical for energy harvesting in mobile electronic devices and wireless sensor nodes under indoor illumination. Multiwalled CNTs are unique one dimensional metallic materials whose conductance show positive temperature dependence [30]. Their electrical conducting properties together with their

Manuscript received October 13, 2013; revised April 3, 2014 and January 29, 2014; accepted July 10, 2014. Date of publication July 25, 2014; date of current version September 4, 2014. This work was supported by the Cambridge University Centre for Advanced Photonics and Electronics under the Strategic Research Initiative and the Nokia-Cambridge Strategic Alliance in Nanoscience and Nanotechnology as part of the Mobile Energy Programme. The work of H. Zhou was supported in part by the National Natural Science Foundation of China under Grant 61204077, and the Shenzhen Science and Technology Innovation Commission (JCYJ20120614150521967). The review of this paper was arranged by Associate Editor A. Martinez.

H. Zhou and F. Tao are with the School of Electronic and Computer Engineering, Peking University Shenzhen Graduate School, National Institute of Standards and Technology, Shenzhen 518055, China (e-mail: zhouh81@pkusz.edu.cn; dddtc2006@gmail.com).

P. Hiralal, A. Nathan, and G. A. J. Amaratunga are with the Center for Advanced Photonics and Electronics, University of Cambridge, Cambridge CB3 0FA, U.K. (e-mail: pv237@cam.ac.uk; an299@cam.ac.uk; gaja1@cam.ac.uk).

A. Ahnood is with the Department of Physics, University of Melbourne, Melbourne 3010, Australia (e-mail: ahnood@gmail.com).

H. E. Unalan is with the Department of Metallurgical and Materials Engineering, Middle East Technical University, Ankara 06800, Turkey (e-mail: unalan@metu.edu.tr).

This paper has supplementary downloadable material available at http://ieeexplore.ieee.org (File size: 1 MB).

Color versions of one or more of the figures in this paper are available online at http://ieeexplore.ieee.org.

Digital Object Identifier 10.1109/TNANO.2014.2343256

available controlled growth techniques have made them suitable building blocks for creating periodic NP structures. We previously reported a core-shell ITO/amorphous silicon/CNT heterojunction cell [25] with short-circuit current enhancement compared to the planar counterpart. This approach facilitates the translation of geometric feature of the CNT array into the morphology of the solar cell creating a three-dimensional thin film device. In practice, amorphous silicon photodiodes are based on p-i-n or n-i-p structure. Conventional p-n diode structure does not work for amorphous silicon due to the short minority carrier lifetime in highly doped layers. Photons absorbed in doped layers are mostly lost due to recombination. In p-i-n or n-i-p structure, the p and n layer creates an internal field (typically more than 10^4 V/cm) which separate the photogenerated electron–hole pairs in the intrinsic layer, and drive the electron and holes drifted towards opposite direction [31]. However, the p and n layer has to be thin (less than 20 nm) enough to let most incoming electrons get absorbed in the intrinsic layer. Here, we further demonstrated the fabrication of a full n-i-p amorphous silicon NP solar cell using metallic multiwalled carbon nanotube arrays as scaffolds, and systematically studied the influence of array spacing on electrical and optical properties of the NP solar cell. Periodic NP solar cell devices based on arrays of CNTs with spacing of 800, 1000, and 2000 nm were fabricated and investigated.

II. Fabrication Process

A periodic array of free standing vertical CNTs was grown on a low doped crystalline Si substrates (1–10 Ω·cm), using patterned catalyst particles as reported in other works [32]. Further details of the growth technique are provided in the supporting information Section S1. Three CNT samples with different spacing of 800, 1000, and 2000 nm were fabricated. On each device, CNTs were grown to cover a total area of 2 mm $\times$ 2 mm. The average length and diameter of the CNTs were approximately 2 μm and 250 nm, respectively.

A layer of chromium (Cr) thin film ($\sim$100 nm), with resistivity in the order of $10^{-5}\Omega$·cm, was thermally evaporated onto the CNTs in order to homogenize the current collector's work function. The Cr was deposited both onto the CNTs and the planar region of the silicon substrate between CNTs to form the back electrode onto which the thin film silicon layers were deposited. The thickness of the Cr thin film on the side walls of CNTs was thinner than the Cr thin film on the flat substrate due to the directional preference of the evaporation technique. The resulting Cr layer increased the CNT diameter to $\sim$300 nm, as shown in the SEM images in Fig. S1, available in the online supplementary material. The c-Si substrate together with CNTs is used as supporting scaffold, which does contribute to the photovoltaic process. The photocurrents were collected through the highly conductive Cr contact. Amorphous Si PV devices with full n-i-p stacks were sequentially deposited in a two-chamber radio frequency plasma enhanced chemical vapour deposition (RF-PECVD) system, with the n- layer deposited first at the bottom of the stack, forming ohmic contact with the Cr electrode [33]. Further information on the deposition condition is provided in the Electronic Supplementary Material. The intrinsic Si layer thickness was set to 300 nm on the planar substrate, and the thicknesses of both doped layers were around 20 nm. CNTs scaffolds control the surface morphology of the PV cell. This coupled with the coated metal thin film provides a transportation path for the photogenerated carriers, while the outer thin film Si forms the shell, where electron–hole pairs are generated and separated. The top indium tin oxide (ITO) contact was sputtered with a target thickness of 80 nm on top of each device. Although it has been reported that p-type a-Si:H/ITO contact is a Schottky type [34], the highly doped p-layer and n-layer can still provide a sufficient built-in potential for photovoltaic process. During ITO deposition, a metal shadow mask was used in defining an open area of 3 mm $\times$ 3 mm, covering the whole CNT grown region. Finally, a reactive ion etching step was used to remove the Si layers outside of the ITO coated region to define the active photovoltaic device with the area of 3 mm $\times$ 3 mm. This etch step precisely defined the device size to 3 mm $\times$ 3 mm. The 2 mm $\times$ 2 mm CNT growth area is located at the center of the whole device. CNT free edges of the device were used for contacting during device characterization in a probe station. The final device structure (Cr-CNT/n-i-p Si/ITO) and its band diagram is schematically presented in Fig. 1(a). A planar control sample without any CNT array was also fabricated alongside the CNT array sample. Although textured front contacts are widely adopted in p-i-n amorphous silicon solar cell technology, the temperature for CNT growth is above 700 °C which has prohibited the use of TCO substrates in our study. In order to examine the contribution of periodic NP s to the overall photovoltaic effect, a planar n-i-p cell is fabricated on a bare Cr coated silicon substrate for comparison. In this case, the deposition sequence for different the layers have kept the same for all the devices, and the amorphous silicon/metal interface are almost identical for planar and NP devices.

The structure of the fabricated devices was investigated using a Zeiss (EVO MA) scanning electron microscopy (SEM). The optical reflectance was measured using an optical fibre reflectance measurement setup (see Fig. S2, available in the online supplementary material) [35] with a freshly deposited chromium film on a silicon substrate used as the reference. The absolute reflected photon number counts were first collected from the fabricated PV samples and the reference samples. The relative reflectance of these samples was obtained by dividing the photon counts of the photovoltaic devices by the reference sample. The electrical performance of the devices, including the dark and light *I–V* characteristics, were characterized in a probe station with electrical noise shield as well as light shield (Cascade probe station) using a semiconductor analyzer (Agilent B1500A). White light emitting diodes (LEDs) were attached to the probe station's microscope to provide illumination intensity of 5 mW/cm^2 (5% of AM1.5 solar intensity, measured using DS-056 Daystar solar meter) for measurement under weak illumination conditions. External quantum efficiency (EQE) of the photovoltaic devices was measured to determine the current produced upon illumination from wavelengths of 400 to 800 nm.

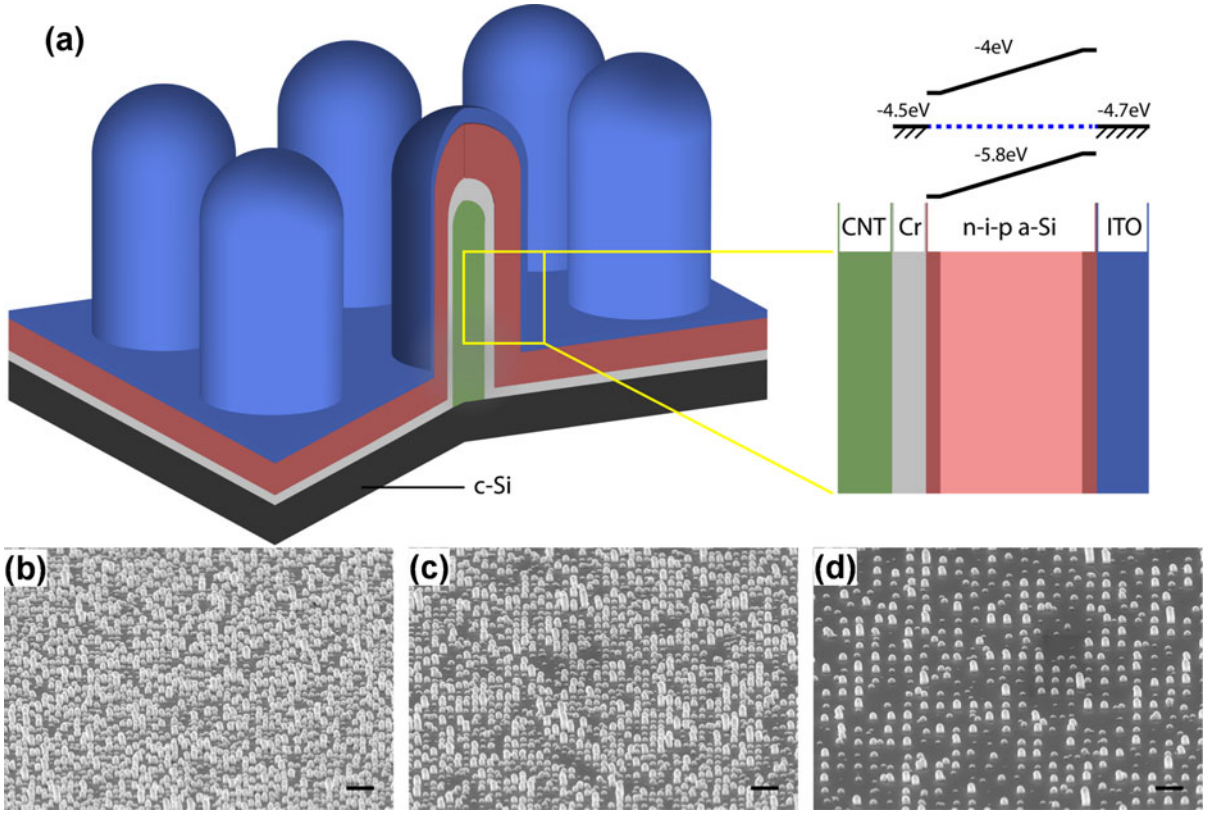

Fig. 1. (a) Schematic of the fabricated NP PV devices, highlighting its cross-sectional structure with n-i-p a-Si:H layers deposited onto Cr coated CNT arrays and its equilibrium band diagrams (vacuum level is not shown). (b) and (c) SEM images of coaxial NP n-i-p Si NP PV devices with CNT arrays spacings of (b) 2000, (c) 1000, and (d) 800 nm. All SEM images are taken at 45° tilted angle. Scale bars correspond to 4 μm.

III. Results and Discussion

SEM images of the coaxial nip devices fabricated using CNT arrays with spacings of 2000, 1000, and 800 nm are provided in Fig. 1(b)–(d), respectively. The fabricated NPs had an average diameter of 750 nm in all the three samples, and were capped by a semispherical dome which formed during deposition. As the CNT array spacing is reduced, the NPs start to merge, as shown in Fig. 1(d) which depicts 800-nm CNT spacing. There was an unintentional variation in the NP length, due to the nonuniformity in the length of CNTs grown in our PECVD setup (see Fig. S1 in supporting information). The CNT growth condition could be further optimized to reduce the variation in the length of the CNTs [36]. In this study, such variation was within the acceptable range as the periodicity of the NPs was maintained. The reflectance spectra for the fabricated NP PV devices are shown in Fig. 2(a). It is evident that all the NP PV devices exhibit much lower reflectance compared to the planar PV device sample. It should be noted that although in the case of planar device, the 80-nm thick ITO layer acted as an antireflection layer, it is only effective over a narrow spectral range, giving the lowest reflection at around 660 nm for the planar sample. In contrast to the planar device, the NP PV devices showed a broader spectrum antireflection behavior, where reduction in the CNT spacing leads to decrease in the intensity of the reflection peaks and valleys. The average reflectance for the 800-nm CNT spacing sample was less than 10%.

At 550-nm illumination wavelength, the reflectance of the NP cell with a spacing of 800 nm was ~5%, and was an order of magnitude smaller compared to that of the planar device (~63%). The surface morphology of the NP with 800-nm spacing resembles that of a moth-eye, where the periodic NPs create a graded refractive index layer that suppresses the reflection of incoming light of a broad spectrum. It is worth to notice that the dome-shape top of the NP was formed automatically during the thin-film deposition on CNT arrays.

Finite difference time domain (FDTD) simulation software (Lumerical Solutions Inc.) was used to verify the origin of antireflection effect in the periodic nanopilllar array. The optical performance of the devices were simulated using the FDTD, where three-dimensional models of Si NP PV devices with three different spacings were constructed using parameters similar to those in the real device (see Fig. S3 and the simulation parameters in Section S3, available in the online supplementary material). Models of NP with flat top and semispherical (dome-shape) top were both constructed. In both cases, NP arrays of three different spacings have shown lower reflectance compared to the planar device in the 400–800 nm range, in line with the experimental results in Fig. 2(a). The contrast between the capping form factor (i.e., flat top versus semispherical top) becomes more evident as the spacing between the NP is reduced. The simulation results showed that NP solar cells with a semispherical top yield better antireflection performance than the flat

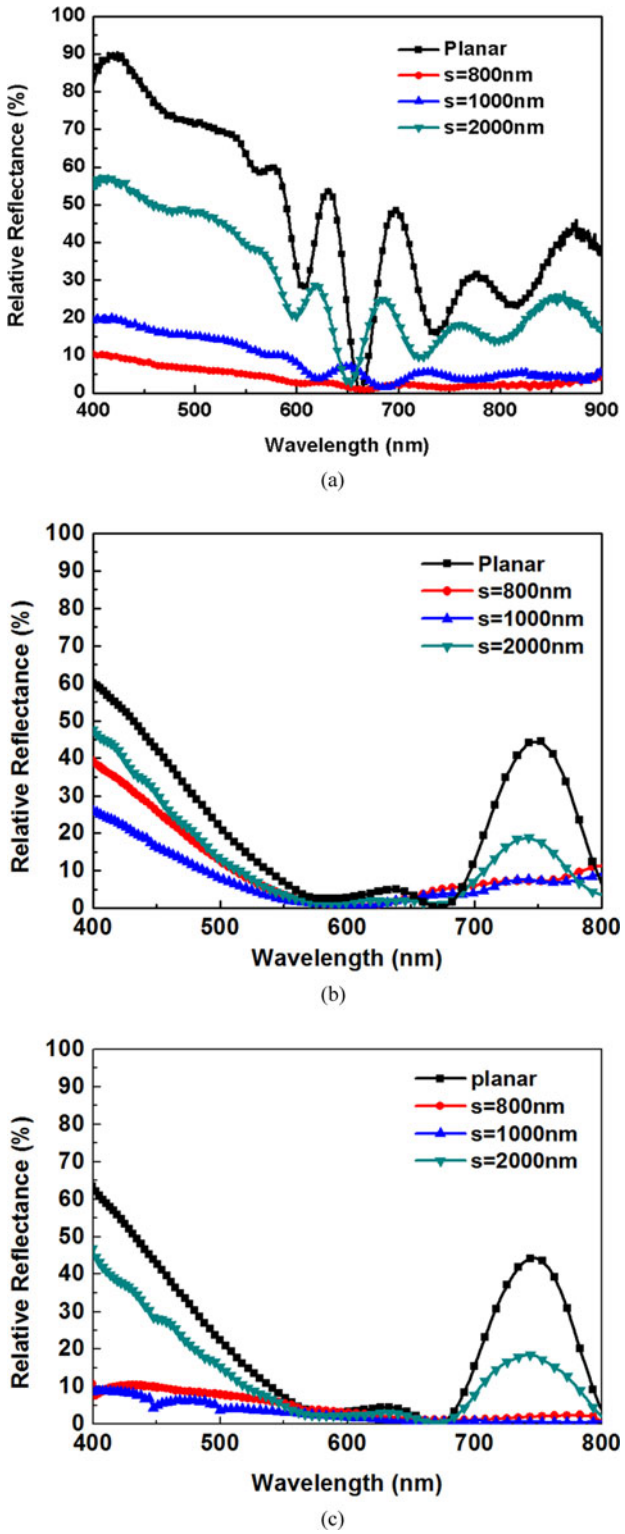

Fig. 2. (a) Measured relative reflectance spectra of NP photovoltaic devices. (b) Simulated reflectance for NP photovoltaic devices with flat top and (c) with semispherical top. The CNTs spacing in the sample is denoted as "s." A chromium thin film (100 nm) on glass was used as reflection reference sample. Spectrum of planar sample is also included.

top counterparts [see Fig. 2(b)] in the CNT spacing ranges of 1000 nm and below. Furthermore, in the case of NPs with a flat top structure, the reflectance of 800-nm CNT spacing is significantly larger than the reflectance for 1000-nm CNT spacing. This behavior is reversed in the case of NP with semispherical top where reflectance at 800-nm spacing is suppressed to a value similar to that of 1000-nm CNT spacing, in line with the experimental results presented in Fig. 2(a), where semispherical top case approximates well to the fabricated nanopilllar solar cells. Overall, the simulation results as well as the experimental data indicate that semispherical top together with dense NPs lead to a 'moth-eye' broadband antireflection effect.

Current density-voltage (J–V) characteristics of the NP photovoltaic devices under weak illumination are depicted in Fig. 3(a). Study on the device performance at low light intensity is valuable for applications such as image sensors for medical imaging and energy harvesting in mobile electronic devices under indoor illumination. Under the short-circuit condition, the short-circuit current density ($J_{\rm SC}$) of NP photovoltaic devices with spacing of 800 (1.15 mA/cm^2) and 1000 nm (1.10 mA/cm^2) outperformed the planar cell (1.06 mA/cm^2). This enhancement is more significant when the nanopilllar devices were reversely biased. Under reverse bias of -0.4 V, the photocurrent density of the NP solar cells with CNT spacing of 800 nm was found to be 1.2 mA/cm^2, much higher than that of the planar device (1.1 mA/cm^2). However, NP device with a spacing of 2000 nm, on the contrary, had the lowest $J_{\rm SC}$ (0.99 mA/cm^2) among all devices, despite its reflectance being lower than that of the planar cell. This can be attributed to the reflection of diffracted light from the 2000-nm CNT NP solar cell. Although generally reduced reflection in photovoltaic devices is associated with enhanced photoabsorption and thus enhanced photocurrent, color dispersion can be observed at the surface of the NP solar cell with 2000-nm spacing. This higher order diffracted light is reflected in an angle that falls outside of the fiber probe's light collection domain and therefore cannot be detected. Therefore, light absorption in the NP solar cell with 2000-nm spacing would not have been enhanced due to diffracted reflections. Diffractive light scattering from periodic arrays is consisted with the published works, and can be eliminated through the use of NPs with spacing that is small enough to become a zeroth-order grating [37]–[40]. For the solar cell applications, the nanopilllar spacing must be smaller than 1000 nm to suppress diffractive scattering. Similar effect have been observed in the moth-eyes [41]. A spacing below 1000 nm would also lead to NP cells with feature sizes in the subwavelength range, resulting in an antireflection structure. Random structures could theoretically offer a maximum absorption enhancement of $4n^2$, which is known as Yablonovitch limit [42]. It is important to note that this limit was derived with assumption that an absorber layer thickness is much larger than the wavelength, which is not achievable for thin films with thickness less than one micrometer. Periodicity in the order of wavelength can help scatter incident light into guided modes in the thin films which enhance light absorption [26]. For periodic gratings, the maximum possible enhancement of $14.5n^2$ derived by Yu *et al.* is achieved at a periodicity of $2/\sqrt{3}\lambda$.[43] Targeting optical enhancement for amorphous silicon thin film at a wavelength

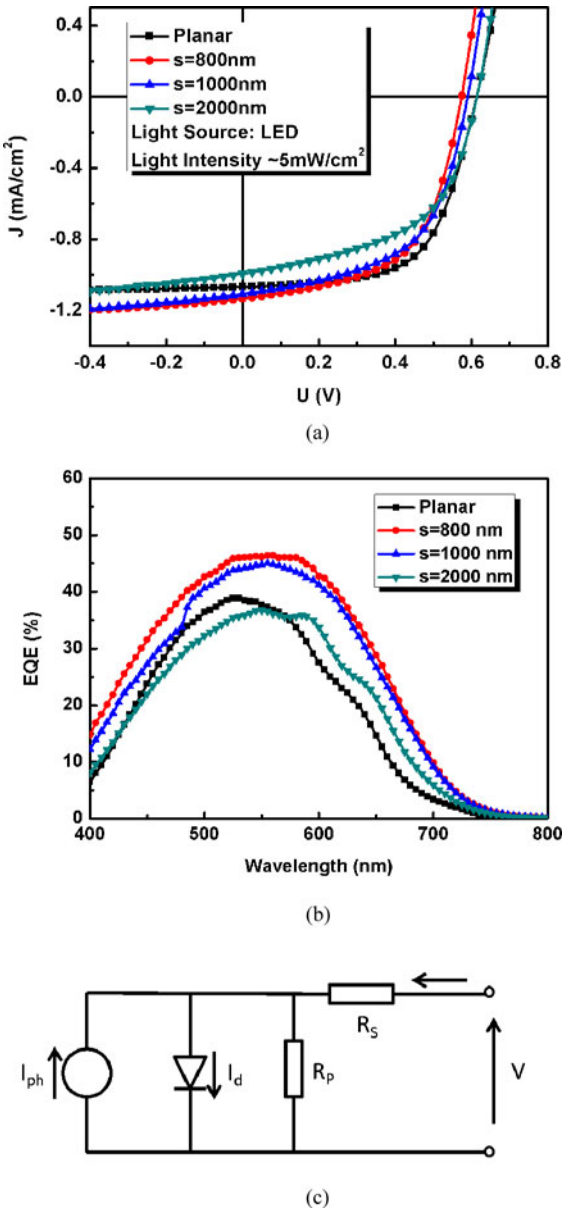

Fig. 3. (a) *J–V* characteristics of NP devices under white LED light (~5 mW/cm2). (b) EQE results of NP PV devices compared to a planar device Results of planar sample are also included. (c) Equivalent circuit diagram of the solar cell.

around 700 nm, the calculated periodicity is ~808 nm, which is close to our dense array with 800-nm CNT spacing.

The $J_{\rm SC}$ enhancement of the NP solar cells obtained under the weak illumination condition is consistent with the EQE measurements depicted in Fig. 3(b). In the measurement wavelength range of 400–800 nm, the NP solar cells with CNT spacings of 800 and 1000 nm yield a higher EQE compared with the planar cell using conventional antireflective coating. The enhancement in the EQE is most pronounced for the NP solar cell with the CNT spacing of 800 nm, particularly at the longer wavelengths region of 600–700 nm. The EQE enhancement was most significant in the long wavelength region (600–700 nm). The enhanced gain at longer wavelength is expected due to enhanced optical absorption from the NP structure which compensates the smaller absorption coefficient of amorphous silicon thin film. On the contrary, in the short wavelength region (400–550 nm), the enhancement of EQE in the nanopilllar cells was less pronounced. The optical enhancement in this region could be offset by the photogenerated carrier loss in the top Si p-layer. It is well known that the carrier lifetimes are short in this heavily doped layer. Most incoming photons in the short wavelength range absorbed by this layer are mostly wasted, negating part of the EQE gain in this region. The PV cell with a spacing of 2000 nm had the lowest EQE values in the short wavelength range (400–570 nm) among all the devices, providing evidence that these CNT arrays have a strong scattering effect on these photons. These EQE results are actually in good agreement with the photocurrent results shown in Fig. 3(a). It should be noted that the intensity of the monochromatic light used for the EQE measurement is significantly weaker than the light intensity used in both the strong illumination measurement and the weak illumination measurement conditions. This leads to EQE results which are in agreement with the photocurrent measurement under weak illumination presented in Fig. 3(a), where the results are dominated by the optical gain in the device and not the recombination.

Despite the increase in $J_{\rm SC}$ of NP photovoltaic devices, the open-circuit voltage ($V_{\rm OC}$) significantly decreased with the increase in the array density as the nanopilllar spacing is reduced from 2000 to 800 nm, from 0.62 to 0.57 V. As a result, the overall efficiency of the NP (s-800 nm) is 0.5% lower than that of the planar device under weak 5-mW/cm^2 illumination. Under AM1.5G (100 mW/cm^2) illumination condition, the drop in $V_{\rm OC}$ [see Fig. 4(a)] with respect to the NP spacing was more significant, reducing from around 0.68 V for the planar cell to 0.53 V for the NP device with a spacing of 800 nm. Similar voltage drop phenomena has been reported on solar cells using dense random forest-like silicon NWs [21], [22].

From the equivalent circuit view, there are a number of factors that could results in the reduction in the $V_{\rm OC}$ of the NP solar cells compared with the planar ones. First, the doped layers on the CNT walls are thinner than the planar regions. Insufficiently thick dope layer can give rise to a reduction in the build in potential of the solar cells, and therefore, a reduction in the $V_{\rm OC}$ of the NP solar cells compared with the planar one. As the density of the NP solar cells are increased with the reduction in the CNT spacing the overall CNT array's $V_{\rm OC}$ decreases further, explaining the reduction in the reduction in the $V_{\rm OC}$ when the CNT spacing is reduced from 2000 to 800 nm. The second effect which governs $V_{\rm OC}$ is the loss of photogenerated carriers due to the recombination, especially at the p/i interface. The enhanced surface area of NP PV device could lead to an overall larger recombination rate than the planar device. Therefore, the $V_{\rm oc}$ drop could be due to the increased carrier recombination at the NP interfaces. The third possible effect which contributes to the reduction in the $V_{\rm OC}$ is the reduction in shunt resistance of NP solar cells. The different growth rate and direction of silicon thin-film solar cells at the intersection between the CNT and planar areas gives rise to microstructural defects which gives rise to shunting behavior [44].

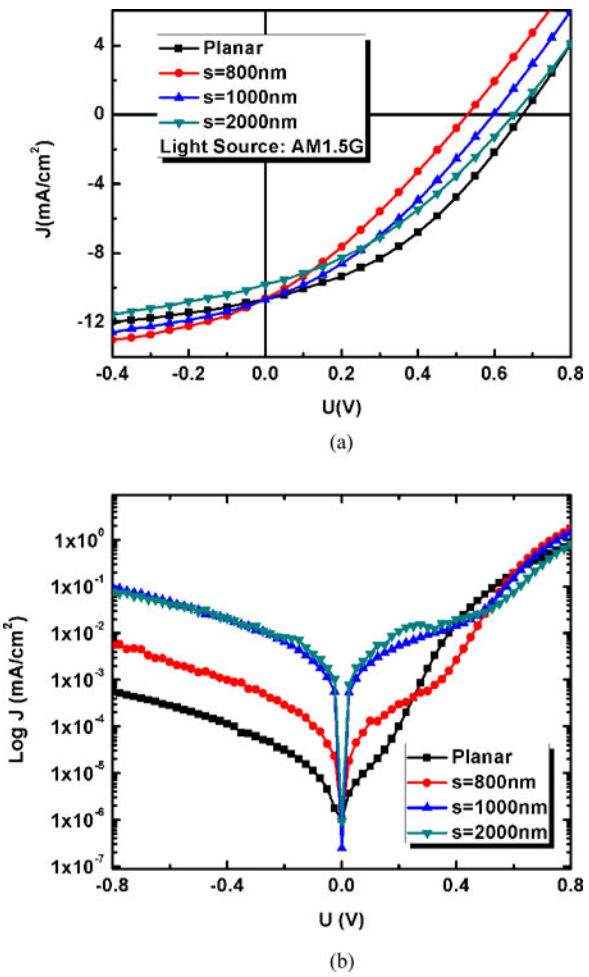

Fig. 4. (a) *J–V* characteristics of NP devices under solar simulator with AM1.5G filter. (b) Semilog plot of dark current density–voltage characteristics of NP PV devices compared to a planar device.

The characteristics of the solar cell under strong illumination intensity provide further evidence to the origins of the $V_{\rm OC}$ behavior. In the case of NP solar cells with CNT spacing of 800 nm, the $V_{\rm OC}$ drops from 0.57 to 0.53 V with the increase in the illumination. This drop is inconsistent with the shunting type defect as well as thin doped layer defects, both of which exhibit a larger $V_{\rm OC}$ with the increase in the illumination intensity. However, in the case of recombination losses, particularly the interfacial recombination losses at p/i interface, the increase in the illumination intensity leads to a higher recombination rate at the interfacial regime which in turn distorts the electric field in the interstice layer, giving rise to a reduction in the built in potential and subsequently the open circuit voltage. The performance of the nanopilllar solar cells are limited by the strong recombination losses, which adversely affects their $J_{\rm SC}$ and the fill factor, offsetting the benefits of the antireflective optical properties gained from the use of the periodic NPs. Thus, the enhancement in $I_{\rm SC}$ observed under the weak illumination condition therefore cannot be translated under the strong illumination condition.

TABLE I
PERFORMANCE PARAMETERS OF PLANAR AND NP PHOTOVOLTAIC DEVICES UNDER LOW LIGHT INTENSITY (5 MW/CM^2)

	$V_{\rm oc}$ (V)	$I_{\rm sc}$ (mA/cm^2)	F.F (%)	η (%)
Planar	0.62	1.06	61.5	8.0
$S = 2000$ nm	0.62	0.99	52.3	6.4
$S = 1000$ nm	0.59	1.10	55.9	7.3
$S = 800$ nm	0.57	1.15	57.2	7.5

TABLE II
IDEALITY FACTOR, REVERSE SATURATION CURRENT, SERIAL AND SHUNT RESISTANCE OF PLANAR AND NP PHOTOVOLTAIC DEVICES

	Planar	800 nm	1000 nm	2000 nm
N	1.7	2.8	5.4	6.9
J_0 (mA/cm^2)	1.55E-6	2.05E-5	1.09E-3	2.28E-3
Rs ($\Omega \cdot$ cm^2)	50	67	71	106
Rp (k$\Omega \cdot$ cm^2)	4320	720	14	21

To further explore the electrical properties of the NPs, we investigated the dark *J–V* characteristics as shown in Fig. 4(b). The diode rectification ratio of the planar cell, defined as the ratio of dark current at $+0.8$ V to dark current at -0.8 V, is in the order of 10^3, significantly larger than the rectification ratios of the NP solar cells at less than 10^2. Although this reduction can be partially attributed to the increase in reverse bias current due to the increase in the active junction area, our calculation suggests that this effect is less one order and cannot fully account for the reduction in the rectification ratio. Therefore, the increase of dark current under reverse bias cannot be solely ascribed to the surface area enhancement of the NPs. Current leakage paths through the solar cells or surface recombination can both lead to the reduction in the rectification ratio. There must be current leakage paths through bulk or surface recombination.

The ideality factors (n), reverse saturation current densities (J_0) and resistances (R_s and R_p) of the NP and planar solar cells are extracted and presented in Table II. The values of the series resistance were approximated by the slope of dark *J–V* curve at 0.7 V. Within a voltage range of 0 to 0.2 V, the dark current was mainly determined by the shunt resistance, value of which was approximated by the slope of the dark *J–V* curve at 0 V. The large series resistance in the NP devices could be ascribed to the thinner ITO layer on the side wall of NPs. The small parallel resistance in the NP solar cell, on the other hand, is suspected to be ascribed to a current leakage path is due to microstructural defects in the silicon thin film at the junction of planar and vertical device areas. The dark *J–V* curve of the NP photovoltaic devices can be viewed as the *J–V* curve of the planar cell superimposed with a current density contribution from a sample with low parallel resistance.

It is well known that stress can induce crystallization of amorphous silicon thin films [45]. In the joint region of the planar and the NP part, the Si thin film has orthogonal growth directions which create stress. This stress could induce nano/microcrystalline silicon regions with boundaries that

introduce high surface and bulk recombination. While mechanisms behind the distortion of the dark *I–V* curves of the NP device requires further studies, at this stage, we note that the ideality factor and the rectification ratio of the NP solar cell with a spacing of 800 nm outperforms other NP photovoltaic devices. This suggests that the electrical performance of the device could be improved with an optimized NP density. As there exists only NPs in the cell with a spacing of 800 nm, the Si layer only covers the sidewalls of CNTs. This gives rise to a limited junction volume between the NP and planar regions, resulting in high shunt resistance. It is clear that the devices could be further improved by a more conformal three-dimensional coating, which should help in reducing the series resistance and increasing the shunt resistance. Systematical studies on the uniformity of the thin films are needed for future improvement.

IV. Conclusion

We present NP-array thin film amorphous Si PV devices using periodic CNT arrays as scaffolds. Our study on the effect of CNT array spacing shows that the periodic NP devices with spacing less than 1000 nm demonstrate 'moth-eye' antireflection behavior, yielding higher photocurrent and better spectral responsivities compared to the planar cells. We also shows that the V_{oc} of NP solar cells is strongly affected by CNT array spacing, due to the higher overall photocarrier recombination associated with enhanced surface area of NPs potentially, especially under high intensity illumination. At the current research stage, these NP array are more suitable for energy harvesting under indoor environment. It is evident that advanced deposition techniques or passivation materials are also required for further development of NP solar cells for outdoor application.

References

[1] J. Zhu, C.-M. Hsu, Z. Yu, S. Fan, and Y. Cui, "Nanodome solar cells with efficient light management and self-cleaning," *Nano Lett.*, vol. 10, no. 6, pp. 1979–1984, Jun. 2010.

[2] M. Vanecek, O. Babchenko, A. Purkrt, J. Holovsky, N. Neykova, A. Poruba, Z. Remes, J. Meier, and U. Kroll, "Nanostructured three-dimensional thin film silicon solar cells with very high efficiency potential," *Appl. Phys. Lett.*, vol. 98, no. 16, p. 163503, 2011.

[3] M. M. Hilali, S. Yang, M. Miller, F. Xu, S. Banerjee, and S. V Sreenivasan, "Enhanced photocurrent in thin-film amorphous silicon solar cells via shape controlled three-dimensional nanostructures," *Nanotechnology*, vol. 23, no. 40, p. 405203, Oct. 2012.

[4] R. Yu, Q. Lin, S.-F. Leung, and Z. Fan, "Nanomaterials and nanostructures for efficient light absorption and photovoltaics," *Nano Energy*, vol. 1, no. 1, pp. 57–72, Jan. 2012.

[5] R. Kapadia, Z. Fan, K. Takei, and A. Javey, "Nanopillar photovoltaics: Materials, processes, and devices," *Nano Energy*, vol. 1, no. 1, pp. 132–144, Jan. 2012.

[6] B. Tian, X. Zheng, T. J. Kempa, Y. Fang, N. Yu, G. Yu, J. Huang, and C. M. Lieber, "Coaxial silicon nanowires as solar cells and nanoelectronic power sources," *Nature*, vol. 449, pp. 885–889, 2007.

[7] N. S. Lewis, "Toward cost-effective solar energy use," *Science*, vol. 315, no. 5813, pp. 798–801, Feb. 2007.

[8] B. M. Kayes, H. A. Atwater, and N. S. Lewis, "Comparison of the device physics principles of planar and radial p-n junction nanorod solar cells," *J. Appl. Phys.*, vol. 97, no. 11, p. 114302, 2005.

[9] J. Zhu, Z. Yu, G. F. Burkhard, C.-M. Hsu, S. T. Connor, Y. Xu, Q. Wang, M. McGehee, S. Fan, and Y. Cui, "Optical absorption enhancement in amorphous silicon nanowire and nanocone arrays," *Nano Lett.*, vol. 9, no. 1, pp. 279–282, Jan. 2009.

[10] E. Garnett and P. Yang, "Light trapping in silicon nanowire solar cells," *Nano Lett.*, vol. 10, no. 3, pp. 1082–1087, Mar. 2010.

[11] O. L. Muskens, J. G. Rivas, R. E. Algra, E. P. A. M. Bakkers, and A. Lagendijk, "Design of light scattering in nanowire materials for photovoltaic applications," *Nano Lett.*, vol. 8, no. 9, pp. 2638–2642, 2008.

[12] L. Hu and G. Chen, "Analysis of optical absorption in silicon nanowire arrays for photovoltaic applications," *Nano Lett.*, vol. 7, no. 11, pp. 3249–3252, Nov. 2007.

[13] K. K. S. Lau, J. Bico, K. B. K. Teo, M. Chhowalla, G. A. J. Amaratunga, W. I. Milne, G. H. McKinley, and K. K. Gleason, "Superhydrophobic carbon nanotube forests," *Nano Lett.*, vol. 3, no. 12, pp. 1701–1705, Dec. 2003.

[14] W. Wu, S. Krishnan, T. Yamada, X. Sun, P. Wilhite, R. Wu, K. Li, and C. Y. Yang, "Contact resistance in carbon nanostructure via interconnects," *Appl. Phys. Lett.*, vol. 94, no. 16, p. 163113, 2009.

[15] Y. Cui and C. M. Lieber, "Functional nanoscale electronic devices assembled using silicon nanowire building blocks," *Sci.*, vol. 291, no. 5505, pp. 851–853, Feb. 2001.

[16] T. J. Kempa, J. F. Cahoon, S.-K. Kim, R. W. Day, D. C. Bell, H.-G. Park, and C. M. Lieber, "Coaxial multishell nanowires with high-quality electronic interfaces and tunable optical cavities for ultrathin photovoltaics," in *Proc. Natl. Acad. Sci. USA.*, vol. 109, no. 5, pp. 1407–1412, Jan. 2012.

[17] K. Wang, J. Chen, W. Zhou, Y. Zhang, Y. Yan, J. Pern, and A. Mascarenhas, "Direct growth of highly mismatched type II ZnO/ZnSe core/shell nanowire arrays on transparent conducting oxide substrates for solar cell applications," *Adv. Mater.*, vol. 20, no. 17, pp. 3248–3253, 2008.

[18] M. Law, L. E. Greene, J. C. Johnson, R. Saykally, and P. Yang, "Nanowire dye-sensitized solar cells," *Nat. Mater.*, vol. 4, no. 6, pp. 455–459, 2005.

[19] H. T. Ng, J. Han, T. Yamada, P. Nguyen, Y. P. Chen, and M. Meyyappan, "Single crystal nanowire vertical surround-gate field-effect transistor," *Nano Lett.*, vol. 4, no. 7, pp. 1247–1252, Jul. 2004.

[20] H. Kang, J. Park, T. Choi, H. Jung, K. H. Lee, S. Im, and H. Kim, "n-ZnO:N/p-Si nanowire photodiode prepared by atomic layer deposition," *Appl. Phys. Lett.*, vol. 100, no. 4, p. 041117, 2012.

[21] H.-D. Um, S. A. Moiz, K.-T. Park, J.-Y. Jung, S.-W. Jee, C. H. Ahn, D. C. Kim, H. K. Cho, D.-W. Kim, and J.-H. Lee, "Highly selective spectral response with enhanced responsivity of n-ZnO/p-Si radial heterojunction nanowire photodiodes," *Appl. Phys. Lett.*, vol. 98, no. 3, p. 033102, 2011.

[22] J. Cho, B. O. Donnell, L. Yu, K. Kim, and I. Ngo, "Sn-catalyzed silicon nanowire solar cells with 4. 9% efficiency grown on glass," *Prog. Photovolt: Res. Appl.*, vol. 21, no. 1, pp. 77–81, 2013.

[23] M. M. Adachi, M. P. Anantram, and K. S. Karim, "Core-shell silicon nanowire solar cells," *Sci. Rep.*, vol. 3, pp. 2–7, Mar. 2013.

[24] T. Paudel, J. Rybczynski, Y. T. Gao, Y. C. Lan, Y. Peng, K. Kempa, M. J. Naughton, and Z. F. Ren, "Nanocoax solar cells based on aligned multiwalled carbon nanotube arrays," *Phys. Status Solidi*, vol. 208, no. 4, pp. 924–927, Apr. 2011.

[25] H. Zhou, A. Colli, A. Ahnood, Y. Yang, N. Rupesinghe, T. Butler, I. Haneef, P. Hiralal, A. Nathan, and G. A. J. Amaratunga, "Arrays of parallel connected coaxial multiwall-carbon- nanotube-amorphous-silicon solar cells," *Adv. Mater.*, vol. 21, pp. 3919–3923, Oct. 2009.

[26] C. Battaglia, C.-M. Hsu, K. Söderström, J. Escarré, F.-J. Haug, M. Charrière, M. Boccard, M. Despeisse, D. T. L. Alexander, M. Cantoni, Y. Cui, and C. Ballif, "Light trapping in solar cells: Can periodic beat random?," *ACS Nano*, vol. 6, no. 3, pp. 2790–2797, Mar. 2012.

[27] H. Butt, T. Butler, Y. Montelongo, R. Rajesekharan, T. D. Wilkinson, and G. A. J. Amaratunga, "Continuous diffraction patterns from circular arrays of carbon nanotubes," *Appl. Phys. Lett.*, vol. 101, no. 25, p. 251102, 2012.

[28] S.-F. Leung, M. Yu, Q. Lin, K. Kwon, K.-L. Ching, L. Gu, K. Yu, and Z. Fan, "Efficient photon capturing with ordered three-dimensional nanowell arrays," *Nano Lett.*, vol. 12, no. 7, pp. 3682–3689, Jul. 2012.

[29] J. Oh, H.-C. Yuan, and H. M. Branz, "An 18.2%-efficient black-silicon solar cell achieved through control of carrier recombination in nanostructures," *Nat. Nanotechnol.*, vol. 7, no. 11, pp. 743–748, Nov. 2012.

[30] T. Yamada, H. Yabutani, T. Saito, and C. Y. Yang, "Temperature dependence of carbon nanofiber resistance," *Nanotechnology*, vol. 21, no. 26, p. 265707, Jul. 2010.

[31] J. Yang, A. Banerjee, and S. Guha, "Amorphous silicon based photovoltaics—From earth to the "' final frontier," *Energy Convers.*, vol. 78, pp. 597–612, 2003.

[32] K. B. K. Teo, M. Chhowalla, G. A. J. Amaratunga, W. I. Milne, D. G. Hasko, G. Pirio, P. Legagneux, F. Wyczisk, and D. Pribat, "Uniform patterned growth of carbon nanotubes without surface carbon," *Appl. Phys. Lett.*, vol. 79, no. 10, p. 1534, 2001.

[33] A. J. Szadkowski, "Implications of the change in work function of chromium by the presence of hydrogen on the properties of electrical contact between chromium and hydrogenated amorphous silicon," *J. Appl. Phys.*, vol. 53, no. 1, p. 557, 1982.
[34] F. Saánchez-Sinencio and R. Williams, "Barrier at the interface between amorphous silicon and transparent conducting oxides and its influence on solar cell performance," *J. Appl. Phys.*, vol. 54, no. 5, p. 2757, 1983.
[35] S. A. Boden and D. M. Bagnall, "Optimization of moth-eye antireflection schemes for silicon solar cells," *Prog. Photovoltaics Res. Appl.*, vol. 18, no. 3, pp. 195–203, May 2010.
[36] J. G. Wen, Z. P. Huang, D. Z. Wang, J. H. Chen, S. X. Yang, Z. F. Ren, J. H. Wang, L. E. Calvet, J. Chen, J. F. Klemic, and M. A. Reed, "Growth and characterization of aligned carbon nanotubes from patterned nickel nanodots and uniform thin films," *J. Mater. Res.*, vol. 16, no. 11, pp. 3246–3253, Jan. 2011.
[37] P. Lalanne and G. M. Morris, "Antireflection behavior of silicon subwavelength periodic structures for visible light," *Nanotechnology*, vol. 8, no. 2, pp. 53–56, Jun. 1997.
[38] G. Mariani, Z. Zhou, A. Scofield, and D. L. Huffaker, "Direct-bandgap epitaxial core-multishell nanopillar photovoltaics featuring subwavelength optical concentrators," *Nano Lett.*, vol. 13, no. 4, pp. 1632–1637, May 2013.
[39] W. H. Southwell, "Pyramid-array surface-relief structures producing antireflection index matching on optical surfaces," *J. Opt. Soc. Am. A*, vol. 8, no. 3, pp. 549–553, 1991.
[40] Y.-F. Huang, S. Chattopadhyay, Y.-J. Jen, C.-Y. Peng, T.-A. Liu, Y.-K. Hsu, C.-L. Pan, H.-C. Lo, C.-H. Hsu, Y.-H. Chang, C.-S. Lee, K.-H. Chen, and L.-C. Chen, "Improved broadband and quasi-omnidirectional anti-reflection properties with biomimetic silicon nanostructures," *Nat. Nanotechnol.*, vol. 2, no. 12, pp. 770–774, Dec. 2007.
[41] S.-Y. Chuang, H.-L. Chen, J. Shieh, C.-H. Lin, C.-C. Cheng, H.-W. Liu, and C.-C. Yu, "Nanoscale of biomimetic moth eye structures exhibiting inverse polarization phenomena at the Brewster angle," *Nanoscale*, vol. 2, no. 5, pp. 799–805, May 2010.
[42] E. Yablonovitch, "Statistical ray optics," *J. Opt. Soc. Am.*, vol. 72, no. 7, p. 899, Jul. 1982.
[43] Z. Yu, A. Raman, and S. Fan, "Fundamental limit of light trapping in grating structures," vol. 18, pp. 366–380, Sep. 2010.
[44] H. Sakai, T. Yoshida, T. Hama, and Y. Ichikawa, "Effects of surface morphology of transparent electrode on the open-circuit voltage in a-Si:H solar cells," *Jpn. J. Appl. Phys.*, vol. 29, no. 4, pp. 630–635, Apr. 1990.
[45] J. Park, S. Kwon, S.-I. Jun, I. N. Ivanov, J. Cao, J. L. Musfeldt, and P. D. Rack, "Stress induced crystallization of hydrogenated amorphous silicon," *Thin Solid Films*, vol. 517, no. 11, pp. 3222–3226, Apr. 2009.

Authors' photographs and biographies not available at the time of publication.